



Nanoindentation creep testing: Advantages and limitations of the constant contact pressure method

Christian Minnert^{1,a)} , Karsten Durst¹

¹Physical Metallurgy, Materials Science Department, Technical University of Darmstadt, Darmstadt, Germany

^{a)}Address all correspondence to this author. e-mail: c.minnert@phm.tu-darmstadt.de

Received: 28 July 2021; accepted: 19 November 2021; published online: 6 December 2021

Different loading protocols have been developed in the past to investigate the creep properties of materials using instrumented indentation testing technique. Recently, a new indentation creep method was presented, in which the contact pressure is kept constant during the creep test segment, similar to the constant stress applied in a uniaxial creep experiment. In this study, the results of constant contact pressure creep tests are compared to uniaxial and constant load hold indentation creep experiments on ultrafine grained Cu and CuAl5. The constant contact pressure method yields similar stress exponents as the uniaxial tests, down to indentation strain rates of 10^{-6} s^{-1} , whereas the constant load hold method results mainly in a relaxation of the material at decreasing applied pressures. Furthermore, a pronounced change in the power law exponent at large stress reductions is found for both uniaxial and constant contact pressure tests, indicating a change in deformation mechanism of ultrafine grained metals.

Introduction

Creep properties have been determined for a long time with standardized, macroscopic test methods (e.g. [1–3]). However, sample and test preparation of these standardized experiments are quite time-consuming. Furthermore, it is not possible to test individual phases such as those found e.g. in Ni-based superalloys using macroscopic test procedures. Macroscopic creep testing methods require relatively large sample volumes, which is critical for the analysis of the creep response in small volumes of e.g. thin coatings [4].

Indentation testing, moreover, allows to perform a multitude of creep tests semi-automatically on a single polished sample surface, which significantly increases the sample throughput. The small volume probed allows the mechanical properties of individual microstructure components or thin films to be investigated [5, 6]. Therefore, various indentation creep and relaxation test procedures have been developed for investigating the local, time-dependent mechanical properties. These test procedures promise to provide results comparable to macroscopic tests [7–14]. However, a direct comparison of macroscopic and indentation loading protocols reveals significant differences.

In an uniaxial creep experiment, the applied stress is kept constant for the entire creep segment and the time-dependent strain and strain rates are analyzed. In the most commonly used

constant load hold (CLH) indentation creep method, the load is kept constant and the time-dependent change of hardness and indentation depth are analyzed. For self-similar pyramidal indenters, the resulting strain gradient distribution below the indent is often interpreted as a constant representative strain whereas the hardness can be understood as a representative stress acting within the plastic zone [15]. Indentation testing results thereby in a complex triaxial stress state and the plastically deformed volume is expanding throughout the experiment as described e.g. by Johnson's expanding cavity model [16, 17]. Moreover, both, hardness and indentation strain rate decline with increasing creep time during a constant load and hold experiment, which is in contrast to uniaxial creep testing.

To overcome the limitations of the constant load and hold test, namely the declining indentation stress and indentation strain rate, we have recently presented a new constant contact pressure (CCP) indentation creep method [11], in which the contact pressure, respectively, the stiffness based hardness [8, 11, 18]:

$$H = \frac{4P\beta^2 E_r^2}{\pi S^2} \quad (1)$$

is kept constant throughout the entire creep segment by controlling P/S^2 , where P is the applied load and S is the contact

stiffness, β is a geometrical constant and E_r is the reduced modulus. The contact stiffness is determined using the continuous stiffness measurement (CSM) technique, where the loading signal is superimposed with an additional sinusoidal dynamic displacement. The contact stiffness is thereby determined at an oscillation frequency of 45 Hz, applying a dynamic displacement amplitude of 2 nm. Based on the contact stiffness, the contact pressure can be easily evaluated by using Eq. 1, which was introduced by Joslin and Oliver [18]. Since the contact stiffness is directly related to the contact area, Eq. 1 can be used to determine directly the contact pressure, assuming a constant and depth independent Young's modulus. This contact pressure, determined at a frequency of 45 Hz, is thus based on the current contact situation and is independent of pile-up or thermal drift effects [8, 11, 18].

During a CCP test, the indenter tip is first indentation strain rate controlled loaded onto the surface up to a predefined load or depth, and then the contact pressure is kept constant, but at a lower level compared to the initial hardness value. To keep the average indentation stress inside the plastic zone (the mean contact pressure) constant, the applied load P has to increase continuously, which is in contrast to uniaxial testing (Fig. 1). The plastic zone thus expands with the increasing load, while the resulting indentation strain rate declines with creep time until a plateau in the indentation strain rate is reached [11].

The contact stiffness, determined during the creep segment is also used to assess the contact depth h_c using Eq. 2 [8]:

$$h = h_c + \frac{\varepsilon P}{S} \quad (2)$$

with indentation depth h , and a geometrical constant $\varepsilon = 0.75$ for a three-sided pyramidal Berkovich indenter. The indentation strain rate $\dot{\varepsilon}_{ind}$ can be defined via Eq. 3:

$$\dot{\varepsilon}_{ind} = \frac{\dot{h}}{h} = \frac{1}{2} \left(\frac{\dot{P}}{P} - \frac{\dot{H}}{H} \right) \approx \frac{1}{2} \frac{\dot{P}}{P} \quad (3)$$

whereas the indentation creep rate is defined as $\dot{\varepsilon}_{ind} = \dot{h}/h$ in the CCP and CLH method.

Another advantage of the CCP test method is that the nanoindenter adjusts the loading rate, in order to keep the contact pressure constant and only has to monitor changes in load or indentation depth vs time in order to determine the strain rate. This allows to assess much smaller strain rates in comparison with constant strain rate (CSR) and strain rate jump (SRJ) experiments, which keep the strain rate constant and allow only a limited variation in indentation strain rate (10^{-1} – 10^{-3} s $^{-1}$). Further details and results of experiments performed with the CCP test methodology on fused silica and ultrafine grained alloys can be found in [11].

The strain rate sensitivity can be analyzed by the strain rate dependent change in deformation resistance or stress (Eq. 4) [7]:

$$m = \frac{d(\ln H)}{d(\ln \dot{\varepsilon}_{ind})} = \frac{d(\ln \sigma)}{d(\ln \dot{\varepsilon}_{uni})} \quad (4)$$

with indentation strain rate $\dot{\varepsilon}_{ind}$ and uniaxial strain rate $\dot{\varepsilon}_{uni}$. The activation volume is associated with the active deformation mechanisms and is given for uniaxial and indentation test by Eq. 5 [7, 8]:

$$m = \frac{1}{n} = \frac{\sqrt{3}kT}{V\sigma_f} = \frac{C\sqrt{3}kT}{VH} \quad (5)$$

with stress exponent n , Boltzman constant k , absolute temperature T and uniaxial flow stress σ_f . It should be noted, that the absolute number of V is not sufficient to describe the complete deformation behavior, since several mechanisms may be active simultaneously. The Berkovich hardness and uniaxial flow stress at a representative strain of about 7.2% can be converted in each other using a strain-rate independent constraint factor C , for metals a constraint factor of 2.8–3 was found [7, 8].

It should be noted, that even if the indentation strain rate plateaus during a constant contact pressure experiment and a steady state in deformation resistance is achieved, the deformation

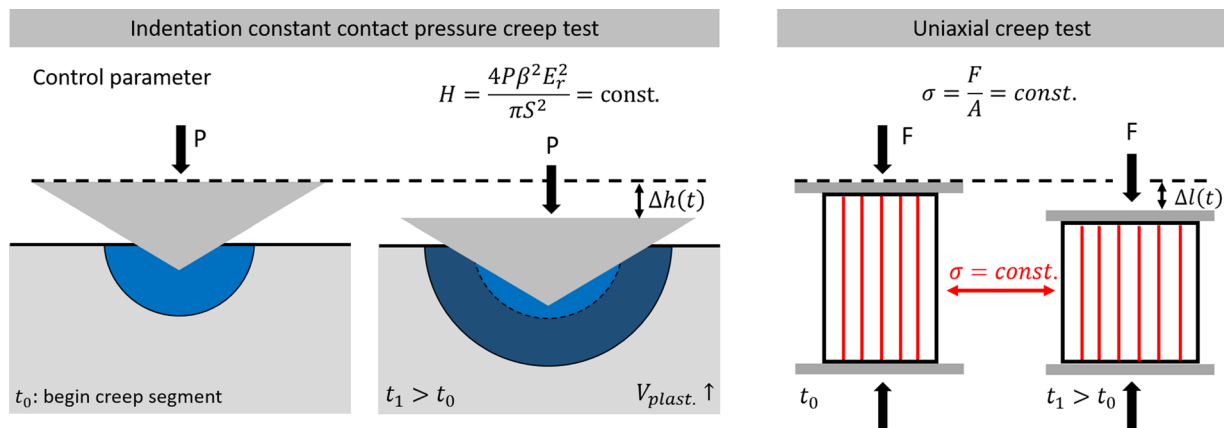


Figure 1: Comparison of the CCP nanoindentation creep method with a conventional uniaxial creep test. Adapted from [11].

microstructure is not necessarily in a steady state. This is caused by a continuous expansion of the plastic zone, whereby fresh, initially undeformed material is continuously being deformed. It is therefore not clear which creep mechanism dictates the minimum creep rate measured during an indentation test and how this relates to the minimum creep rate found in uniaxial creep experiments.

Comparing with literature, it should be noted that the CCP test protocol is quite similar to uniaxial stress dip tests, in which the sample is first loaded to a certain strain level and then partially unloaded, until the desired stress level is reached. Subsequently, the reduced stress is kept constant until the end of the experiment, analyzing the transient creep behavior [19–27]. Stress dip tests have been used in literature to investigate the materials response at different stress levels and a quasi-constant microstructure [25, 28–32], by Blum et al. e.g. [19–24, 31, 32] and Milička e.g. [25–27]. It has been observed that the resulting creep rate immediately after a stress drop depends on the magnitude of stress reduction which can be related to a changing deformation behavior.

Furthermore, Sun et al. used uniaxial stress dip tests inside a synchrotron to analyze the dynamic recovery behavior of nanocrystalline Ni and NiFe alloys [31, 32]. They found that the balance between dislocation nucleation and annihilation and thus the dislocation density changes depending on the amount of stress reduction during a stress dip test. At high stress levels and forward deformation, grain boundaries can act as sources but also as sinks for the dislocations. Strong stress reductions cause an inversion of the dislocation motion (backward deformation), leading dislocations to annihilate in the grain boundaries. This relaxation process leads to a reduction of the defect density and thus to a softening of the material. Thus, the equilibrium dislocation density correlates with the applied stress [20, 31–33].

A review on deformation mechanism of nanocrystalline and ultrafine grained fcc metals like Ni or Cu can be found in [8, 34–38]. The time-dependent deformation behavior of materials is strongly influenced not only by the homologous temperature and the applied stress, but also by loading history and the microstructure, respectively [20–22, 24, 25, 31, 32, 37–42].

From our previous publication [11] a few open questions remained, related to the contact situation after the indentation stress reduction, as well as for a possible change in deformation mechanism of ultrafine grained (UFG) materials. A pronounced increase in the strain rate sensitivity exponent was found for UFG CuZn30 after large indentation stress reductions, leading to low creep rates. It was not fully clear, which maximum indentation stress reductions are possible for a CCP test and if the observed changes in indentation strain rate sensitivity at low indentation stress levels and large contact pressure reductions are caused by the contact situation, or a

loading history effect, or if the enhanced strain rate sensitivity is indicative of a change in deformation mechanisms.

In the following, the long-term CCP indentation creep methodology is presented with respect to maximum indentation stress reduction and load history effects. The results of the CCP tests are compared to SRJ, as well as CLH indentation creep experiments. Furthermore, uniaxial compression SRJ experiments as well as stress dip tests were carried out on macroscopic compression samples of UFG Cu and a binary UFG Cu alloy with 5 wt% Al.

The UFG microstructures were generated by a semi-constraint high pressure torsion (HPT) process. More detailed information on sample processing and test parameters can be found in “Materials and methods” section. UFG Cu-alloys have been used as reference materials as they can be easily produced via a HPT deformation and show already a significant creep deformation at room temperature. In addition, good data sets on strain rate sensitivities and stress exponents are already available for Cu [33, 37, 38, 43–53] as well as for the investigated CuAl5 alloy investigated [53]. Furthermore, UFG materials do not show a pronounced indentation size effect and are thus nicely suited for indentation creep testing. The hardness is thus nearly independent of the indentation depth and data recorded at different indentation depths can be easily compared. This is in contrast to single crystalline materials, where an indentation size effect also needs to be considered [54].

Results and discussion

Indentation CCP testing

The CCP test procedure consists of two test segments, the initial loading with a constant indentation strain rate (here up to an indentation depth of 500 nm) and the subsequent creep segment where the contact pressure is kept constant (here for 0.8 h). Different contact pressures have been applied by varying the ratio of P/S^2 , where the partial unloading at the beginning of the CCP segment was done in a single step. The load–displacement relationship for CCP tests on CuAl5 applying four different contact pressure reductions is shown in Fig. 2a. In total, the contact pressure was varied in eight different stages between 3.04 and 2.40 GPa (Fig. 2d). At the beginning of the creep segment (Fig. 2a), the indentation control is switched from strain rate control to a constant contact pressure control based on Eq. 1. Doing so, it is apparent that the slope of the load–displacement (Fig. 2a), or load–time data (Fig. 2b), is significantly dropping, when reducing the contact pressure. The P/S^2 ratio is adjusted at the beginning of the creep segment (Fig. 2c) to set the desired contact pressure (Eq. 1) and then kept constant until the end of the experiment.

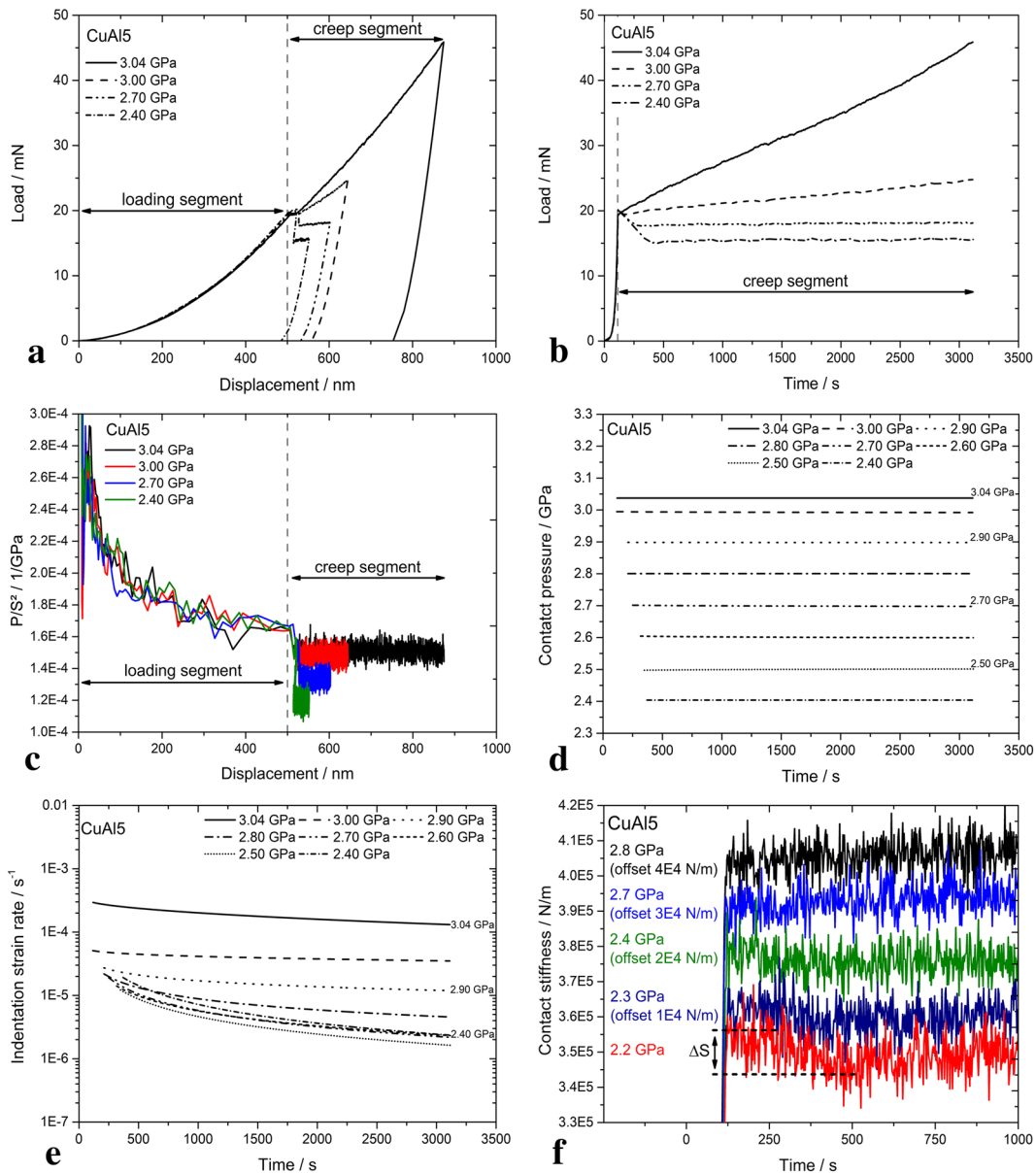


Figure 2: Indentation CCP tests on CuAl5 applying a single unloading event. In (a) the load vs. displacement, in (b) the load vs. time, (c) the P/S^2 ratio vs. displacement, (d) the applied contact pressures vs. time, (e) indentation strain rate vs. time and (f) the contact stiffness vs. time is plotted for a single partial unloading event at the beginning of the CCP test segment. The individual stiffness curves are each shifted by an offset of $1E4$ N/m for a better visibility.

A reduction in contact pressure results in a smaller increase in indentation depth during the creep segment (Fig. 2a). Based on the displacements, the resulting indentation creep strain rates are plotted in Fig. 2e. Here it is clear that both the indentation depth and the indentation strain rate declines with a reduction in indentation contact pressure. The corresponding data for Cu are shown in the Supplementary (S1). This data is later on (Sect. 3.3) used for a comparison with the uniaxial test results.

To analyze the maximum allowable indentation stress reduction, the contact stiffnesses for different contact pressures are shown in Fig. 2f. For low contact pressures (2.2–2.4 GPa) a slight decrease of up to 3.1% in S (Fig. 2f) can be found for $H=2.2$ GPa in the beginning of the creep segment. Furthermore, an apparent increase in the indentation strain rate (not shown) was found for these low contact pressures, which cannot be justified physically and the test were discarded from a further analysis.

The exact reasons for this behavior are not fully clear, but the indenter could potentially lose contact during unloading, also due to the dynamic oscillation of the indenter tip. As a result of the, albeit marginal, unloading, the contact stiffness may no longer be determined correctly [55]. A pronounced decrease in S or at least a significant increase of its scattering would be an indication for contact issues if the tip would lose the contact temporarily due to the load reduction and the additional dynamic displacement (CSM technique). The scattering is independent of the applied pressure, however, a large reduction in contact pressure, can lead to changes in the contact situation and the material behavior could change from fully plastic to elastic-plastic deformation.

In this study and our previous publication on UFG Cu alloys and fused silica [11], the contact pressure could be reduced by approx. 12% (fused silica) to 37% (UFG Cu) (reference value at 0.01 s^{-1}). For CuAl5, the contact pressure (Eq. 1) of 2.4 GPa, corresponding to a reduction of 25%, represents the lower limit. A detailed study of the indentation profiles is also given there.

Load history effect

It is unclear whether the time-dependent deformation behavior is affected by the magnitude of sudden contact pressure reduction at the beginning of the creep segment. Therefore, additional

CCP tests were carried out on CuAl5 in which the contact pressure was reduced incrementally in order to investigate a possible load history effect.

The corresponding load–displacement curves as well as the contact pressure and depth as a function of time are plotted in Fig. 3a, b and c. Up to six successively decreasing contact pressures with a reduction in contact pressure of 0.1 GPa, and 0.2 GPa were applied in the two test series.

A decline in S at very low contact pressures can also be observed with the incremental test method (Fig. 3d), comparable to the original procedure (single unloading, Fig. 2f). The contact stiffness is thus exclusively affected by the reduction of the contact pressure in relation to the initial value at the end of the loading segment. The resulting indentation strain rates for the different contact pressures are compared in Fig. 5b to each other.

Uniaxial constant stress testing

The results of the uniaxial constant stress tests on CuAl5 are shown in Fig. 4. In Fig. 4a, the stress strain response of tests with and without partial unloading segments are plotted. The samples were loaded up to total strains of 3%, reaching a saturation stress. Larger plastic strains caused shear failure of

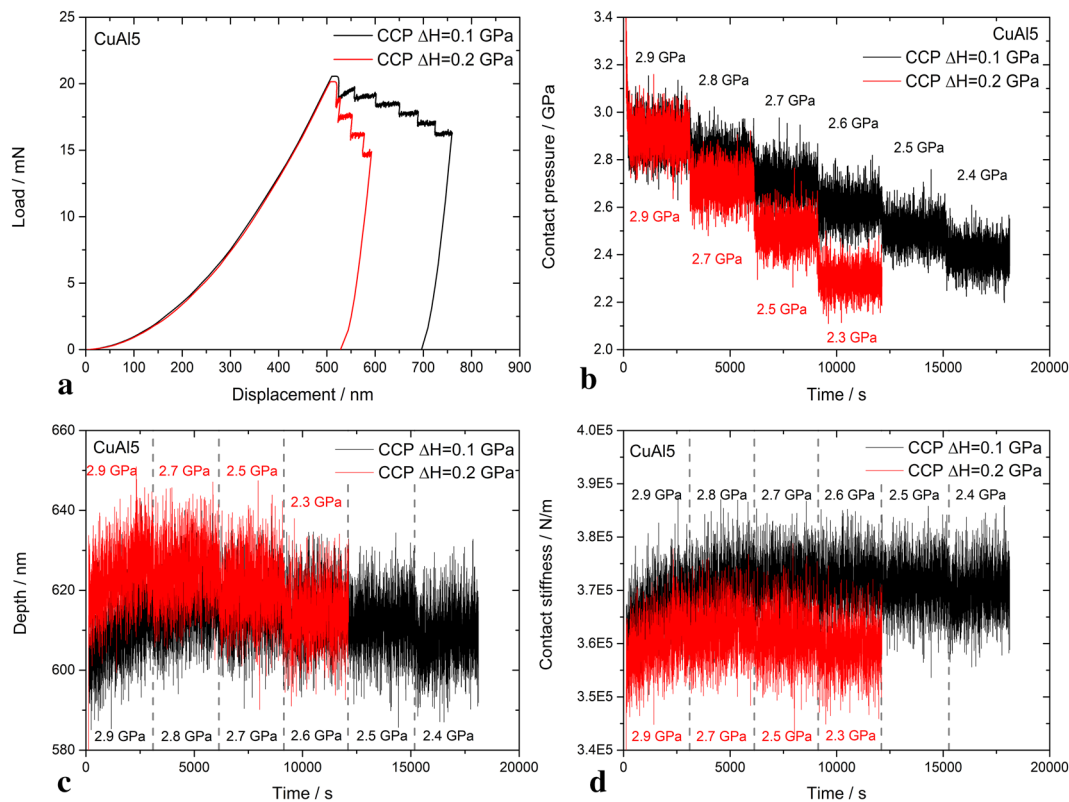


Figure 3: Indentation CCP tests on CuAl5 applying multiple partial unloading events. In (a) the load vs. displacement, in (b) the raw contact pressure vs. time, (c) the corrected indentation depth vs. time and (d) the contact stiffness vs time is plotted.

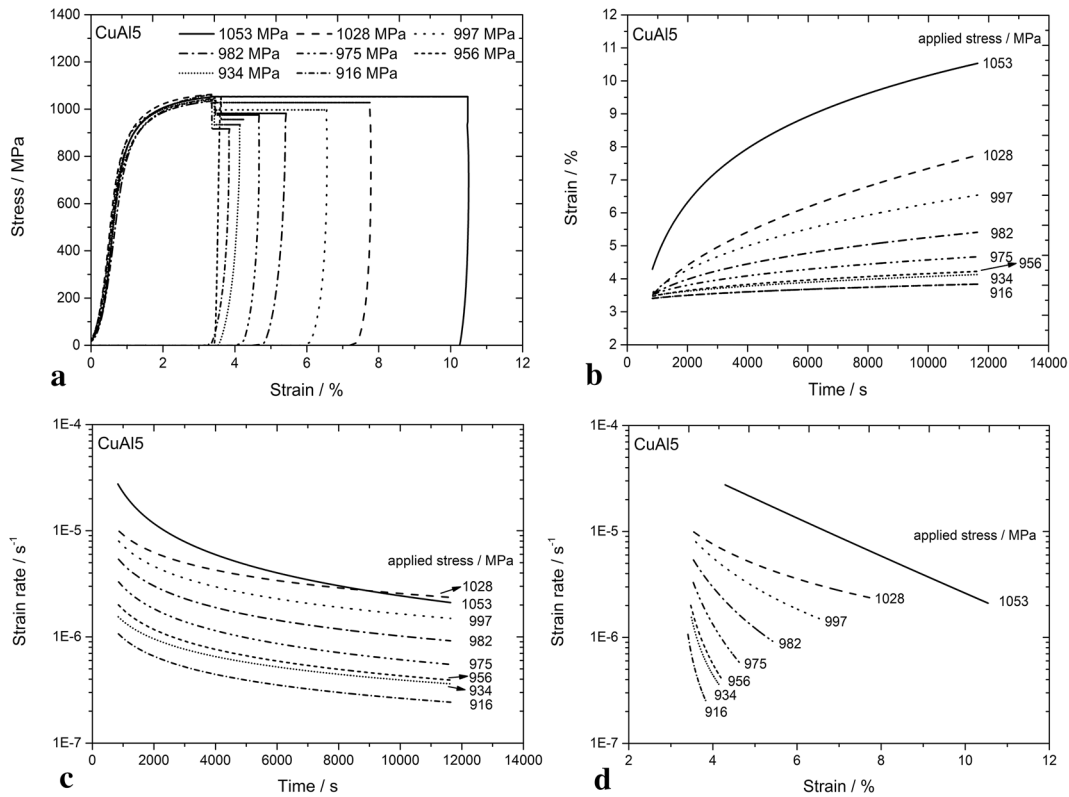


Figure 4: Uniaxial constant stress tests on CuAl5 with partial unloading at the beginning of the creep segment: stress vs. strain (a), strain vs. time (b), strain rate vs. time (c) and strain rate vs. strain (d).

the specimens and could not be applied. The partial unloading was done in displacement control. In the following creep segment, the engineering stress is kept constant for 10,800 s (3 h), resulting in a time dependent creep deformation as shown in Fig. 4b. The resulting creep strain rate as a function of test time and total strain is illustrated in Fig. 4c, d.

It is evident that the resulting strain and strain rate strongly depend on the applied stress level. For constant stress levels or small stress reductions, a high creep strain as well as a high strain rate can be observed during the test period (Fig. 4c). In contrast, a larger stress reduction results in a very low forward deformation of the sample and thus a low creep strain rate. However, a steady state creep condition is not reached during the experiment as the strain rate is continuously decreasing with the applied strain as illustrated in Fig. 4d. The uniaxial stress strain diagrams for Cu can be found in the supplementary (S2). Cu exhibits a similar behavior as CuAl5, except that the strain rate as a function of strain shows saturation at large stress reductions and large strains. The material approaches a steady state behavior.

Comparison of strain rate sensitivity

The results of nanoindentation experiments (CSR, SRJ, CCP and CLH) are plotted in Fig. 5a for Cu and in Fig. 5b for CuAl5, whereas the results of the uniaxial tests (SRJ and constant stress) for Cu and CuAl5 are plotted in Fig. 5c, d respectively. The CSR data were determined in the initial loading segment of CCP tests, prior to partial unloading, and presented for comparison. The data from CCP tests was averaged over the last 500 s of the individual creep segments (between 2500 and 3000 s for CCP tests with a single unloading event). Data from constant stress tests were averaged in the creep segment between 2500 and 3000 s.

The data of the CSR, SRJ and CCP nanoindentation and uniaxial experiments agree well with each other and show two distinct regimes in the deformation behavior, with a lower strain rate sensitivity exponent in the high and a higher strain rate sensitivity exponent in the lower stress regime. The observed transition from the high to the low stress regime takes places at strain rates of about $10^{-5} - 10^{-6} \text{ s}^{-1}$ for both uniaxial and indentation

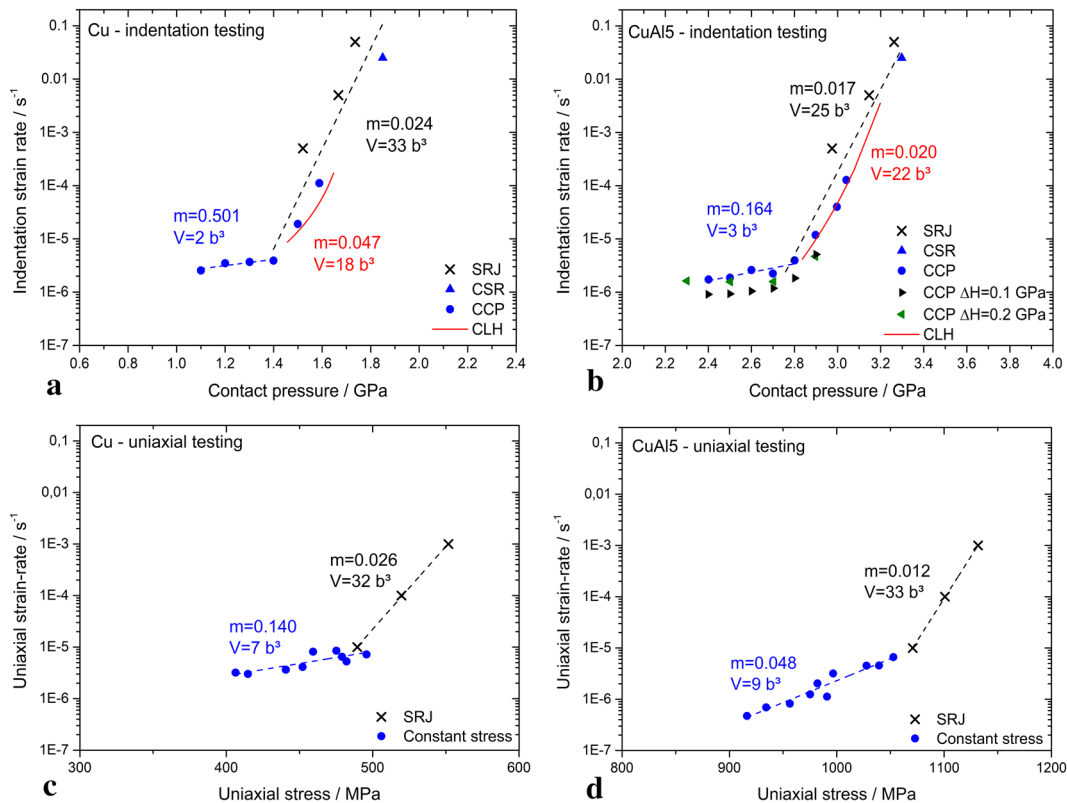


Figure 5: Comparison of the stress dependent equivalent strain rates from nanoindentation (a, b) and uniaxial experiments (c, d) on UFG Cu (left column) and UFG CuAl5 (right column). The CCP creep data was averaged over the last 500 s of the creep segments. Data from constant stress tests were averaged in the creep segment between 2500 and 3000 s.

test approaches. The observed transition in the deformation behavior is thus not a testing artefact of the CCP test method, but clearly results from a change in the deformation mechanism in the tested UFG Cu and UFG CuAl5. In Fig. 5b, also the results of the incremental unloading ($\Delta H = 0.1 - 0.2$ GPa; black and green triangles) are shown in comparison to the results of CCP tests with a single unloading increment (blue circles). All three test series on CuAl5 (Fig. 5b) agree with each other and a history effect can thus be excluded for the current testing results.

In the high stress regime, a strain rate sensitivity value of $m = 0.024$ was obtained for UFG Cu (Fig. 5a) by nanoindentation CCP, CSM and SRJ tests, which agrees with the exponent $m = 0.026$ from the uniaxial strain rate jump tests (Fig. 5c). Both values are in good agreement with literature data of 0.009–0.031 [43–48, 51, 53]. CLH tests results in $m = 0.047$ which is significantly larger than literature values. For UFG CuAl5, (Fig. 5b, d), SRS parameter of 0.012–0.017 (SRJ) and CCP tests) were found which are smaller by a factor of two than previously reported values of 0.024–0.026 [53] determined by SRJ indentation tests. The SRS coefficient determined by CLH tests is 0.020 and therefore comparable with the indentation SRJ/CCP data set ($m = 0.017$). The results of CLH experiments follow to a certain extend the data from SRJ, CSR and CCP data. However there, a

continuous decline in indentation strain rate and contact pressure is found, leading to slightly larger strain rate sensitivity exponents compared to CCP, CSM and SRJ tests.

In the low stress regime, however, significantly larger m values in the range of 0.140–0.501 could be determined for UFG Cu by uniaxial constant stress and CCP indentation tests, respectively. The SRS has therefore increased by a factor of up to 21. A similar, but clearly less pronounced, trend was also observed for CuAl5, where m values of 0.048–0.164 were determined. The CLH experiments did not show the observed transition found in the other experiments after a test duration of 3000 s. A similar behavior was also observed by Yang et al. for relaxation tests on nanostructured Cu [38].

The corresponding activation volumes were calculated using Eq. 5 and the material specific Burgers vectors b [56]. The activation volumes determined in the high stress regime from SRS and CCP tests are quite similar for Cu ($V_{Cu} = 24 - 26b^3$), while V from CLH tests is lower at $18b^3$ (Fig. 5a). For CuAl5, V of 12–20 b^3 were found with very similar values from the indentation tests of $17b^3$ and $22b^3$. Activation volumes larger than $10b^3$ indicate that dislocation cross slip is the dominant deformation mechanism [57]. In contrast, V in the range of 2–9 b^3 were calculated for the low stress regime, with only minor differences

between the activation volumes from uniaxial constant stress and indentation CCP tests. The deformation behavior in the high stress regime is, thus, related to nucleation and motion of dislocations, where dislocation annihilation and grain boundary mediated processes becomes dominant in the low stress regime [37, 38, 57].

The calculated activation volumes only represent an average value and provide only limited information on the actual material behavior as several deformation mechanisms can be active at the same time. This is moreover true, since a steady state condition is not achieved and other transition mechanism, like grain coarsening could influence the calculated values. A detailed discussion of the deformation processes including microstructural influences will be prepared for a separate publication.

A direct comparison of different data sets determined by indentation and compression experiments are given in Fig. 6. We would like to point out that the uniaxial constant stress tests are only to be used for comparison with indentation tests. We are aware that the selected creep times are not sufficient to reach a steady state condition (e.g. Fig. 4c, d). However, uniaxial tests were performed in a similar manner to CCP tests but there are clear differences.

Hardness values were converted to equivalent uniaxial stresses using constant constraint factors of 2.8 for CuAl5 and 3 for Cu. The direct comparison of the indentation and uniaxial tests shows a good correlation for UFG Cu and the high stress regime of CuAl5. In the low stress regime of CuAl5, deviations between the data sets occur.

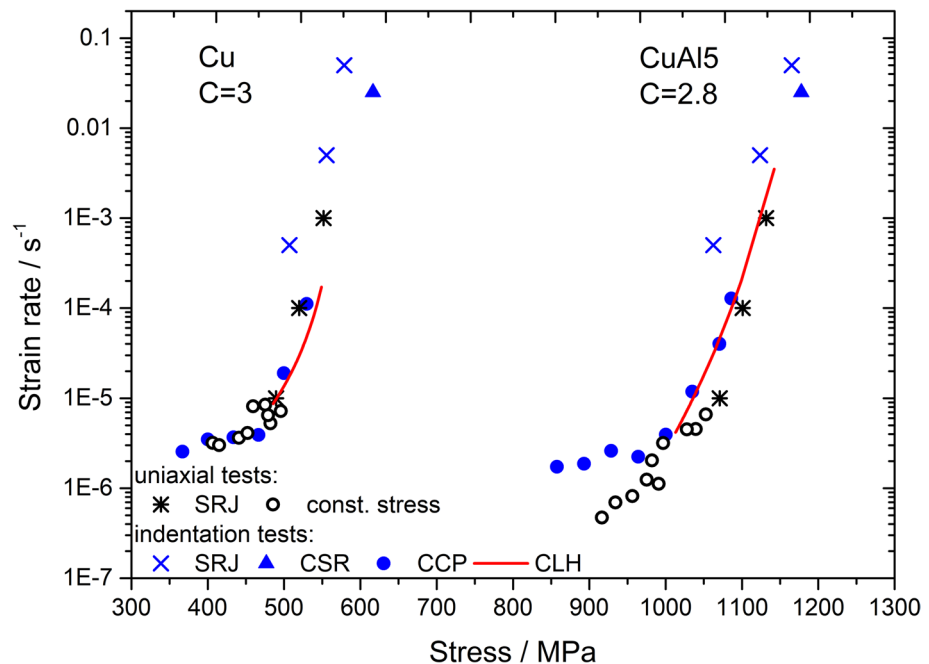
In CCP experiments, the average representative strain is constant, since a Berkovich indenter with a self-similar

geometry has been used whereas the probed volume increases with testing time. In contrast, the specimen volume is constant in a uniaxial test, but the applied strain increases continuously. The stress reductions are comparable for both test procedures but the absolute stresses within the plastic zone underneath the indenter are way higher than in the compression samples. Unstable microstructures are susceptible to high stresses, therefore changes in the microstructure like grain coarsening, are more likely to occur in the case of indentation tests than in a compression test [58–60].

Relaxation processes potentially assisted by grain growth is expected to occur particularly with UFG Cu as observed by Maier-Kiener et al. [53] during nanoindentation testing, while alloying Al leads to a pinning effect of the grain boundaries and thus to a more stable microstructure of CuAl5. This also becomes clear from the course of the strain rate as a function of time, respectively, strain. While the strain rate of UFG Cu (Online Fig. 10c, d) is in a kind of steady state, the decrease of the strain rate of CuAl5 (Fig. 4c, d) is still significant.

In CuAl5, the change in strain rate sensitivity or deformation mechanism takes place at similar stress reductions but is more pronounced for CCP indentation tests. Relaxation processes driven by the inversion of the dislocation motion during the stress dip is dominant for uniaxial testing while a slight grain coarsening is expected to occur during indentation testing [53] due to the higher indentation stresses and the indentation stress gradient within the plastic zone below the indenter.

Figure 6: Comparison of the results from indentation and uniaxial experiments performed on UFG Cu (a) and UFG CuAl5 (b).



Advantages and limitations of the CCP method

The results from CCP tests revealed two deformation regimes for the UFG Cu and UFG CuAl5 alloy. This is similar to the results from uniaxial tests from this work and literature show a similar course as the CCP data [37, 42].

In the newly developed CCP method, the contact pressure within the plastic zone is kept constant by controlling P/S^2 . The results (Fig. 5), are thus comparable to conventional uniaxial creep tests where the stress is kept constant, even at very low strain rates. The expansion of the plastic zone is much more pronounced than in a CLH test [11]. This is however compensated by a simultaneously, continuous increase in the applied load (Fig. 2a, b). In consequence, previously undeformed material is continuously being absorbed by the expanding plastic zone (Fig. 1). The material microstructure and plastic zone thus is never in a steady state condition, even though a steady state in contact pressure is achieved. However, also the uniaxial does not show a steady state behavior for the used testing conditions. A significant extension of the creep time and a temporally constant microstructure would be necessary to achieve this condition. Comparing the development of the creep rates of CCP and uniaxial tests (Figs. 2e and 4c), it is also noticeable that the minimum creep rate is reached much faster during the CCP than the uniaxial experiments.

The maximum possible stress reduction, i.e. the minimum contact pressure that can be applied during the CCP creep segment, correlates with S . In case of large contact pressure reductions (Fig. 2f), a slight drop in contact stiffness is indicative of changes in the contact situation and the reliability of the corresponding creep data is questionable.

The material response immediately after indentation stress reduction does not necessarily correspond to the actual creep behavior as investigated by Blum et al. e.g. [19–24, 31, 32] and Milička e.g. [25–27] using uniaxial stress dip tests. It has been observed that the resulting creep rate immediately after a stress drop depends on the magnitude of stress reduction which can be related to a changing deformation behavior. Small stress reductions causing dislocation glide and dislocation generation. Relaxation processes play a dominant role for large stress reductions.

Relaxation processes are caused by large stress reductions as the direction of dislocation motion can be reversed and dislocations will annihilate at grain boundaries. This can lead to a negative strain rate immediately after the stress drop, since the material response after partial unloading is determined by the net flow (forward and backward flow) of dislocations. However, with increasing test duration, dislocation nucleation will take place again due to the steadily progressing deformation. The dislocation density is changing until an equilibrium of dislocation nucleation and annihilation processes are

established. The resulting long-term deformation rate is thus related to the final, stress dependent dislocation density [19, 20, 24, 31, 32].

In this study, no significant differences were observed between the single and incremental partial unloading experiments (Fig. 5b). However, the data are not reliable as soon as the contact stiffness decreases during partial unloading event. This represents the limiting factor for the reduction of the contact pressure. The upper contact pressure limit is given by the maximum loading rate, which is limited by the control loops of the device.

Furthermore, the higher contact depths when applying multiple contact pressures in succession significantly did not affect the resulting creep rates. This demonstrates the robustness of the method dealing with long testing times and high contact stiffnesses.

Conclusions

The recently developed constant contact pressure (CCP) indentation creep method was successfully validated by macroscopic compression tests. For this purpose, macroscopic SRJ tests as well as long-term constant stress creep experiments as well as nanoindentation CCP, SRJ and CLH tests were performed to determine the strain rate sensitivity of UFG Cu and CuAl5 as processed by high pressure torsion.

It could be demonstrated that the CCP method provides reliable creep data and strain rate sensitivity exponents at indentation strain rates down to about 10^{-6} s^{-1} whereas a high and low stress regime can be distinguished. In the high stress regime, a low strain rate sensitivity is observed compared to the low stress regime. The difference in strain rate sensitivity between the two regimes is more pronounced for UFG Cu in comparison to the UFG CuAl5 solid solution. Here, the deformation behavior is dominated by dislocation annihilation and grain boundary mediated processes. Furthermore, it could be shown that the well-established CLH method is more similar to a relaxation than a creep test. It gives thus deviating results to uniaxial creep experiments especially at very low strain rates. Applying several partial unloading events during a single CCP experiment does not affect the material's response (no history effect), as only the long term creep behavior was analyzed. The smallest achievable contact pressure is determined by the contact situation. Large reductions of the contact pressure lead to a reduction of the contact stiffness. The contact is then no longer fully plastic, which means that the elastic properties of the material influence the results and thus the correct creep behavior is no longer described correctly. The CCP method opens up the possibility of determining the creep properties of individual phases of materials under constant indentation stress conditions. The method is therefore ideally suited to analyze strain

rate dependencies and stress exponents at very low indentation strain rates, which cannot be achieved by any other indentation creep method. Interestingly, the indentation strain rate reaches an approximate constant value much faster than in uniaxial tests, which significantly reduces the testing time. This is an advantage especially for testing at elevated temperatures.

Materials and methods

Experiments were performed on an ultrafine grained CuAl alloy containing 5 wt% Al (purchased from Wieland-Werke AG, Germany) as well as on technical pure Cu.

Sample processing

The UFG microstructures were generated by severe plastic deformation (SPD) using a semi-constrained high pressure torsion press (Walter Klement GmbH, Austria). Therefore, discs with a diameter 20 mm and an initial height of 4.5 mm (approx. 3.3 mm after HPT processing) were deformed applying a compressive force of 1450 kN (pressure of approx. 4.5 GPa) and a rotational speed of 1 rpm until 25 revolutions were completed. The high degree of deformation applied to the material during HPT processing results in homogeneous grain refinement throughout the specimen. The upper anvil was actively cooled to dissipate some of the energy generated by plastic deformation in order to achieve a fine final grain size.

Afterwards, rectangular bars were cut out of the HPT samples, lathed and cut into compression specimens. This procedure is exemplarily shown in Fig. 7. The final cylindrical compression samples had a diameter of 2.5 mm and a length of 3.125 mm (aspect ratio of 1:1.25). The remaining sections of the HPT samples (Fig. 7c, left and right sections) were grinded and subsequently metallographically prepared using different diamond suspensions with particles sizes of 6, 3 and 1 μm . An

oxide particle suspension (colloidal silica, particle size 0.04 μm) with additional ferrinitrate was subsequently used for the final (vibrational) fine polishing.

The resulting grain sizes after HPT processing were analyzed using a high-resolution scanning electron microscope (Mira3, Tescan, Czech) in backscattered electron (BSE) contrast imaging mode (Fig. 8) and a line intercept method. The grain sizes were analyzed at about the half radius ($r = 5 \text{ mm}$) of the HPT disc in order to investigate a representative microstructure. The analysis yields average grain sizes of 425 nm for Cu and 133 nm for CuAl5.

Nanoindentation testing

Nanoindentation experiments were performed with a G200 (Keysight, USA) indentation system equipped with a diamond Berkovich tip (Synton-MDP, Switzerland). The system was calibrated according to Oliver and Pharr [61, 62] using fused silica as reference material.

Strain rate jump tests according to Maier et al. [7] were performed in order to determine the strain rate sensitivity in the indentation strain rate range between ($\dot{P}/P = 0.05 - 0.0005 \text{ s}^{-1}$). Additional long term creep tests were carried out using the constant load hold (CLH) [8] and the recently developed constant contact pressure (CCP) method [11].

In both creep test methods, strain rate controlled loading occurs in the first test segment until a penetration depth of 500 nm is reached, followed by creep segment. In case of the CLH method, the applied load is hold constant during the creep time of 3000 s (0.8 h). In contrast, a continuously loading takes place in the creep segment of the CCP method in order to keep the previously selected contact pressure constant. The creep segment for the CCP tests lasted 3000 s. An indentation strain rate of 0.025 s^{-1} was applied in the initial, constant strain rate loading segment of both, CLH and CCP experiments.

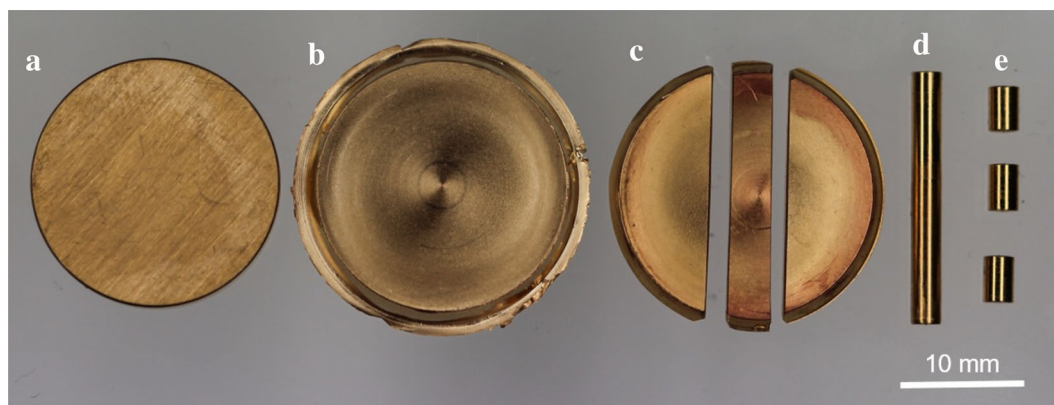


Figure 7: Sample Processing: (a) undeformed HPT sample, (b) sample after HPT processing, (c) cutted rectangular bar, (d) lathed bar and (e) final compression samples.

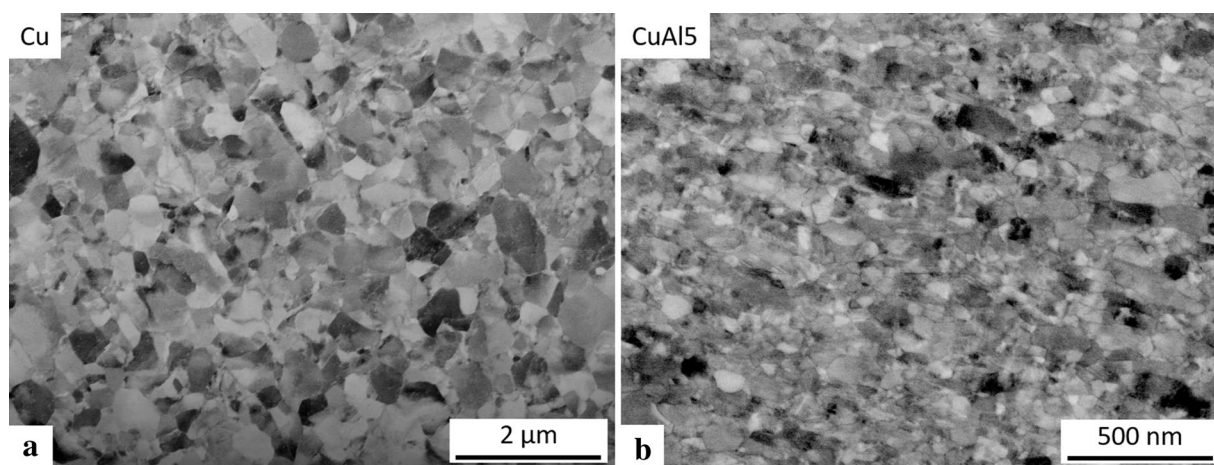


Figure 8: BSE images of (a) UFG Cu and (b) UFG CuAl5 after HPT processing.

In all three methods, the contact stiffness is continuously recorded and used for the calculation of the drift independent and pile-up corrected hardness, respectively, contact pressure according to Eq. 1. Therefore, a dynamic displacement of 2 nm was applied with a dynamic frequency of 45 Hz.

Compression testing

Compression tests were performed using a universal testing device (Instron, Type 5967, USA) equipped with a 30 kN load cell and carbide punches. All compression experiments were carried out inside a closed cabinet in order to reduce the impact of thermal drift on the test results. The cross-sectional area was assumed to be constant.

Compression strain rate jump tests were carried out applying strain rates of 10^{-3} – 10^{-5} s⁻¹.

Additional compression experiments where the stress was hold constant were performed. The creep/constant stress segment started once an approximately constant stress level had been reached. A pyramidal Berkovich indenter generates a representative plastic strain of about 7.2% inside the plastic zone. This rather large plastic strain could not be achieved during compression testing due to shear fracture.

In the constant stress (creep) experiments, the stress level was varied at the beginning of the creep segment similar to the nanoindentation CCP method by changing the applied load. The partial unloading during these stress dip tests were performed displacement controlled with an unloading rate of 5 μm/s. The constant stress tests lasted 3 h.

Acknowledgments

The authors thank Dr. Achim Kuhn (Wieland-Werke AG, Germany) for providing the CuAl5 solid solution alloy as well as Dr. Enrico Bruder and Leonie Frohnapfel for experimental support. Deutsche Forschungsgemeinschaft (DFG) is gratefully

acknowledged for financial support within the project No. 326946902.

Funding

Open Access funding enabled and organized by Projekt DEAL.

Data availability

The data are available upon reasonable request from the corresponding author (C.M.).

Declarations

Conflict of interest The authors declare no conflict of interests.

Open Access

This article is licensed under a Creative Commons Attribution 4.0 International License, which permits use, sharing, adaptation, distribution and reproduction in any medium or format, as long as you give appropriate credit to the original author(s) and the source, provide a link to the Creative Commons licence, and indicate if changes were made. The images or other third party material in this article are included in the article's Creative Commons licence, unless indicated otherwise in a credit line to the material. If material is not included in the article's Creative Commons licence and your intended use is not permitted by statutory regulation or exceeds the permitted use, you will need to obtain permission directly from the copyright holder. To view a copy of this licence, visit <http://creativecommons.org/licenses/by/4.0/>.

Supplementary Information

The online version contains supplementary material available at <https://doi.org/10.1557/s43578-021-00445-6>.

References

1. DIN, *DIN EN ISO 204:2018 Metallic Material—Uniaxial Creep Testing in Tension—Method of Test* (2018).
2. ASTM, *E139-11 Standard Test Methods for Conducting Creep, Creep-Rupture, and Stress-Rupture Tests of Metallic Materials* (2018)
3. DIN, Part 005: Uninterrupted creep and stress-rupture testing, in *DIN EN 2002-005 Aerospace Series—Test Methods for Metallic Materials* (2007)
4. S.J. Bull, Nanoindentation of coatings. *J. Phys. D* **38**(24), R393–R413 (2005)
5. K. Durst, M. Göken, Micromechanical characterisation of the influence of rhenium on the mechanical properties in nickel-base superalloys. *Mater. Sci. Eng. A* **387–389**, 312–316 (2004)
6. W.D. Nix, Elastic and plastic properties of thin films on substrates: nanoindentation techniques. *Mater. Sci. Eng. A* **234–236**, 37–44 (1997)
7. V. Maier et al., Nanoindentation strain-rate jump tests for determining the local strain-rate sensitivity in nanocrystalline Ni and ultrafine-grained Al. *J. Mater. Res.* **26**(11), 1421–1430 (2011)
8. V. Maier et al., An improved long-term nanoindentation creep testing approach for studying the local deformation processes in nanocrystalline metals at room and elevated temperatures. *J. Mater. Res.* **28**(9), 1177–1188 (2013)
9. P.S. Phani, W. Oliver, A direct comparison of high temperature nanoindentation creep and uniaxial creep measurements for commercial purity aluminum. *Acta Mater.* **111**, 31–38 (2016)
10. P.S. Phani, W. Oliver, G. Pharr, On the measurement of power law creep parameters from instrumented indentation. *JOM* **69**(11), 2229–2236 (2017)
11. O. Prach et al., A new nanoindentation creep technique using constant contact pressure. *J. Mater. Res.* **34**(14), 2492–2500 (2019)
12. D. Matschkal-Amberger et al., New flat-punch indentation creep testing approach for characterizing the local creep properties at high temperatures. *Mater. Des.* **183**, 108090 (2019)
13. P. Baral et al., A new long-term indentation relaxation method to measure creep properties at the micro-scale with application to fused silica and PMMA. *Mech. Mater.* **137**, 103095 (2019)
14. P. Baral et al., Indentation creep vs indentation relaxation: a matter of strain rate definition? *Mater. Sci. Eng. A* **781**, 139246 (2020)
15. D. Tabor, *The Hardness of Metals* (Clarendon Press, Oxford, 1951)
16. K.L. Johnson, The correlation of indentation experiments. *J. Mech. Phys. Solids* **18**(2), 115–126 (1970)
17. K.L. Johnson, K.L. Johnson, *Contact Mechanics* (Cambridge University Press, Cambridge, 1987)
18. D.L. Joslin, W.C. Oliver, A new method for analyzing data from continuous depth-sensing microindentation tests. *J. Mater. Res.* **5**(1), 123–126 (1990)
19. W. Blum et al., Two mechanisms of dislocation motion during creep. *Acta Metall.* **37**(9), 2439–2453 (1989)
20. W. Blum, P. Eisenlohr, F. Breutingger, Understanding creep—a review. *Metall. Mater. Trans. A* **33**(2), 291–303 (2002)
21. W. Blum, P. Eisenlohr, J. Hu, Interpretation of unloading tests on nanocrystalline Cu in terms of two mechanisms of deformation. *Mater. Sci. Eng. A* **665**, 171–174 (2016)
22. W. Blum, K. Durst, Kinetics of deformation and recovery of nanocrystalline Ni studied by stress reductions (2016)
23. W. Blum et al., Strain rate contribution due to dynamic recovery of ultrafine-grained Cu–Zr as evidenced by load reductions during quasi-stationary deformation at 0.5 Tm. *Metals* **9**(11), 1150 (2019)
24. R. Kapoor et al., Creep transients during stress changes in ultrafine-grained copper. *Scr. Mater.* **54**(10), 1803–1807 (2006)
25. K. Milička, Constant structure creep in metals after stress reduction in steady state stage. *Acta Metall. Mater.* **41**(4), 1163–1172 (1993)
26. K. Milička, Constant structure experiments in high temperature primary creep of some metallic materials. *Acta Metall. Mater.* **42**(12), 4189–4199 (1994)
27. K. Milička, Constant structure creep experiments on aluminium. *Kovove Mater* **49**, 307–318 (2011)
28. D. Caillard, J.L. Martin, *Thermally Activated Mechanisms in Crystal Plasticity*. Pergamon Materials Series, vol. 8, ed. R.W. Cahn (2003).
29. W. Osthoff et al., Creep and relaxation behavior of Inconel-617. *Nucl. Technol.* **66**(2), 296–307 (1984)
30. M.E. Kassner, Chapter 2—five-power-law creep, in *Fundamentals of Creep in Metals and Alloys*, 3rd edn., ed. by M.E. Kassner (Butterworth-Heinemann, Boston, 2015), pp. 7–102
31. Z. Sun et al., Dynamic recovery in nanocrystalline Ni. *Acta Mater.* **91**, 91–100 (2015)
32. Z. Sun et al., Grain size and alloying effects on dynamic recovery in nanocrystalline metals. *Acta Mater.* **119**, 104–114 (2016)
33. Y. Liu et al., Room temperature nanoindentation creep of nanocrystalline Cu and Cu alloys. *Mater. Lett.* **70**, 26–29 (2012)
34. C.L. Wang et al., Creep of nanocrystalline nickel: a direct comparison between uniaxial and nanoindentation creep. *Scr. Mater.* **62**(4), 175–178 (2010)
35. R.S. Kottada, A.H. Chokshi, Low temperature compressive creep in electrodeposited nanocrystalline nickel. *Scr. Mater.* **53**(8), 887–892 (2005)
36. W.M. Yin et al., Creep behavior of nanocrystalline nickel at 290 and 373 K. *Mater. Sci. Eng. A* **301**(1), 18–22 (2001)
37. X.-S. Yang et al., Time-, stress-, and temperature-dependent deformation in nanostructured copper: creep tests and simulations. *J. Mech. Phys. Solids* **94**, 191–206 (2016)

38. X.-S. Yang et al., Time, stress, and temperature-dependent deformation in nanostructured copper: stress relaxation tests and simulations. *Acta Mater.* **108**, 252–263 (2016)
39. W. Blum, Creep of crystalline materials: experimental basis, mechanisms and models. *Mater. Sci. Eng. A* **319–321**, 8–15 (2001)
40. M.A. Meyers, A. Mishra, D.J. Benson, Mechanical properties of nanocrystalline materials. *Prog. Mater. Sci.* **51**(4), 427–556 (2006)
41. M.A. Meyers, A. Mishra, D.J. Benson, The deformation physics of nanocrystalline metals: experiments, analysis, and computations. *JOM* **58**(4), 41–48 (2006)
42. Y.-J. Wang, A. Ishii, S. Ogata, Transition of creep mechanism in nanocrystalline metals. *Phys. Rev. B* **84**(22), 224102 (2011)
43. G.T. Gray et al., Influence of strain rate & temperature on the mechanical response of ultrafine-grained Cu, Ni, and Al-4Cu-0.5Zr. *Nanostruct. Mater.* **9**(1), 477–480 (1997)
44. Y. Wang, E. Ma, Temperature and strain rate effects on the strength and ductility of nanostructured copper. *Appl. Phys. Lett.* **83**(15), 3165–3167 (2003)
45. Y. Li, X. Zeng, W. Blum, Transition from strengthening to softening by grain boundaries in ultrafine-grained Cu. *Acta Mater.* **52**(17), 5009–5018 (2004)
46. Q. Wei et al., Effect of nanocrystalline and ultrafine grain sizes on the strain rate sensitivity and activation volume: fcc versus bcc metals. *Mater. Sci. Eng. A* **381**(1), 71–79 (2004)
47. S. Cheng et al., Tensile properties of in situ consolidated nanocrystalline Cu. *Acta Mater.* **53**(5), 1521–1533 (2005)
48. J. Chen, L. Lu, K. Lu, Hardness and strain rate sensitivity of nanocrystalline Cu. *Scr. Mater.* **54**(11), 1913–1918 (2006)
49. H. Chandler, A comparison between steady state creep and stress relaxation in copper. *Mater. Sci. Eng. A* **527**(23), 6219–6223 (2010)
50. W. Blum et al., Deformation resistance in the transition from coarse-grained to ultrafine-grained Cu by severe plastic deformation up to 24 passes of ECAP. *Mater. Sci. Eng. A* **528**(29), 8621–8627 (2011)
51. T. Suo et al., Compressive behavior and rate-controlling mechanisms of ultrafine grained copper over wide temperature and strain rate ranges. *Mech. Mater.* **61**, 1–10 (2013)
52. J. Hu et al., Plastic deformation behavior during unloading in compressive cyclic test of nanocrystalline copper. *Mater. Sci. Eng. A* **651**, 999–1009 (2016)
53. V. Maier-Kiener et al., Influence of solid solution strengthening on the local mechanical properties of single crystal and ultrafine-grained binary Cu–Al_x solid solutions. *J. Mater. Res.* **32**(24), 4583–4591 (2017)
54. W.D. Nix, H. Gao, Indentation size effects in crystalline materials: a law for strain gradient plasticity. *J. Mech. Phys. Solids* **46**(3), 411–425 (1998)
55. B. Merle et al., Experimental determination of the effective indenter shape and ϵ -factor for nanoindentation by continuously measuring the unloading stiffness. *J. Mater. Res.* **27**(1), 214–221 (2012)
56. K. Edalati et al., Influence of dislocation–solute atom interactions and stacking fault energy on grain size of single-phase alloys after severe plastic deformation using high-pressure torsion. *Acta Mater.* **69**, 68–77 (2014)
57. M. Monclús, J. Molina-Aldareguia, *High Temperature Nanomechanical Testing*. Handbook of Mechanics of Materials, ed. by C.H. Hsueh, S. Schmauder, C.-S. Chen, K.K. Chawla, N. Chawla, W. Chen, Y. Kagawa (2018).
58. K. Zhang, J. Weertman, J. Eastman, Rapid stress-driven grain coarsening in nanocrystalline Cu at ambient and cryogenic temperatures. *Appl. Phys. Lett.* **87**(6), 061921 (2005)
59. S. Brandstetter et al., Grain coarsening during compression of bulk nanocrystalline nickel and copper. *Scr. Mater.* **58**(1), 61–64 (2008)
60. W. Chen et al., Mechanically-induced grain coarsening in gradient nano-grained copper. *Acta Mater.* **125**, 255–264 (2017)
61. W.C. Oliver, G.M. Pharr, An improved technique for determining hardness and elastic modulus using load and displacement sensing indentation experiments. *J. Mater. Res.* **7**(6), 1564–1583 (1992)
62. W.C. Oliver, G.M. Pharr, Measurement of hardness and elastic modulus by instrumented indentation: advances in understanding and refinements to methodology. *J. Mater. Res.* **19**(1), 3–20 (2004)